

The Application of Normal Stress Reduction Function in Tilt Tests for Different Block Shapes

Dong Hyun Kim¹ · Ivan Gratchev¹ · Maw Hein¹ · Arumugam Balasubramaniam¹

Received: 5 July 2015 / Accepted: 20 April 2016 / Published online: 29 April 2016
© Springer-Verlag Wien 2016

Abstract This paper focuses on the influence of the shapes of rock cores, which control the sliding or toppling behaviours in tilt tests for the estimation of rock joint roughness coefficients (JRC). When the JRC values are estimated by performing tilt tests, the values are directly proportional to the basic friction of the rock material and the applied normal stress on the sliding planes. Normal stress obviously varies with the shape of the sliding block, and the basic friction angle is also affected by the sample shapes in tilt tests. In this study, the shapes of core blocks are classified into three representative shapes and those are created using plaster. Using the various shaped artificial cores, a set of tilt tests is carried out to identify the shape influences on the normal stress and the basic friction angle in tilt tests. The test results propose a normal stress reduction function to estimate the normal stress for tilt tests according to the sample shapes based on Barton's empirical equation. The proposed normal stress reduction functions are verified by tilt tests using artificial plaster joints and real rock joint sets. The plaster joint sets are well matched and cast in detailed printed moulds using a 3D printing technique. With the application of the functions, the obtained JRC values from the tilt tests using the plaster samples and the natural rock samples are distributed within a reasonable JRC range when compared with the measured values.

Keywords Rock cores · Shape correction function · Tilt tests · JRC · Basic friction angles

List of symbols

a	Radius of major axis of ellipse
b	Radius of minor axis of ellipse
a_e	Effective area of contact surface
α	Intersection angle between sliced plane and the centre of cylinder
β	Tilting angle when sliding occurs
b_r	Width of rectangular sample
c_1, c_2, c_3	Constants of quadratic function
d_m	Distance of the centre of mass from the centre of sliding plane
e	Eccentricity of block geometry
h_m	Height of centre of mass from sliding plane
h_p	Height of parallelogram shape sample
h_r	Height of rectangular sample
Q	Weight of block
q_{\max}	Maximum vertical stress at base
q_{\min}	Minimum vertical stress at base
$q_{n_{\max}}$	Maximum normal stress at base
$q_{n_{\min}}$	Minimum normal stress at base
x	Width of contact region

1 Introduction

The joint roughness coefficient (JRC) is a useful parameter which is used to estimate the shear strength of discontinuities (Barton and Choubey 1977; Barton and Bandis 1980; ISRM 1978). The JRC value is generally determined by the comparison of rock surface profiles with typical roughness profiles (ISRM 1978). However, this visual observation is often subjective, and thus, the results are highly dependent on the investigator's experience. This

✉ Dong Hyun Kim
d.kim.gc@gmail.com

¹ Griffith University, Gold Coast, QLD, Australia

might be a reason why Barton and Choubey (1977) suggested tilt or push tests to estimate JRC values.

The relatively simple procedure of a tilt test has made it a popular tool that has been used by several researchers (Cawsey and Farrar 1976; Hencher 1976; Baumgartner and Stimpson 1979; Bruce et al. 1989; Alejano et al. 2012; González et al. 2014). Cawsey and Farrar (1976) reported that tilt tests provided better simulations of sliding behaviour of rock samples than direct shear tests and noted that tilt tests had the advantage of using samples of different sizes. However, Barton and Choubey (1977) pointed out some limitations of tilt tests and recommended that only surfaces with $JRC < 8$ should be used. Consequently, due to the sample irregularity, uneven surfaces of drilled cores are not preferable for tilt testing (Wines and Lilly 2003).

Another factor that needs to be considered is tilt tests, which requires a relatively low range of normal stresses. For example, Barton (2008) reported that the normal stress can be as low as 0.001 MPa. As shown in his earlier work, the length-to-thickness ratio of samples for tilt tests was approximately 4 (Barton and Choubey 1977). Corresponding to the background of Barton's works, the cutting job may be required for shaping the samples to apply the normal load uniformly as well (NGI 2004). However, the sawing process is difficult for small-sized core pieces, and careful control is required so as not to break the specimens in the sampling procedure.

The influences of sample shapes on sliding and toppling behaviour have been studied focusing on a simple square rigid body (Bray and Goodman 1981; Sagaseta 1986; Alejano et al. 2012). These studies theoretically classified the failure modes of blocks on tilting planes using the width-to-height ratio of rectangular blocks. Generally, in the case of the specimens of core joints, the ratio between the height and width of samples and the tilting angles may be more difficult to measure than rectangular blocks in the laboratory. It is also difficult to measure the normal stress distributions at the bases of the various cylinders due to the size and shape variation in the unique cylinder bodies. These different forms of normal stress distribution have a strong influence on the basic friction angles of the rock. Overall, the reliability of JRC estimation using tilt tests largely depends on the application of appropriate normal stress and basic friction angles.

In this study, the influence of block shapes on normal stress distribution is firstly investigated by stress analyses using a theoretical method of eccentrically loaded foundation. Secondly, the influences of core shapes on basic friction angles and normal stresses are investigated by performing a series of tilt tests using flat surface plaster samples. Finally, this experimental study proposes shape correction functions that can be used to estimate the normal stresses and basic friction angles according to the sample

shapes. In order to verify the shape correction functions, JRC values which are obtained from tilt tests using matched plaster joint sets and natural rock samples are compared with the measured values.

2 Theoretical Consideration

2.1 Simplified Shapes of Core Samples

The shapes of rock pieces obtained from serial core samples are affected by the orientations of joint structures of rock mass. Several mechanical fractures are also created through boring procedures. If tilt tests are performed using matched joint sets of drilled cores without sawing procedures for shaping the rock samples, the pieces of cores have various shapes of truncated cylinders based on the distributions of joint sets. In this study, assuming the intersections of joint sets with drilled cores, the geometries of the core pieces are simplified as shown in Fig. 1. This geometry classification using the three cylinder shapes which are right cylinder, wedged cylinder, and truncated cylinder only covers the cases when the intersections between joints in the drill core are clearly identified. The employed joint sets are the combinations of a slanted joint and a horizontal joint.

These shapes can be described in two dimensions as triangle, trapezoid, parallelogram, and rectangular shapes. With the variations in cutting angle (α), the shapes of the 2D geometries vary from an acute angle to a right angle.

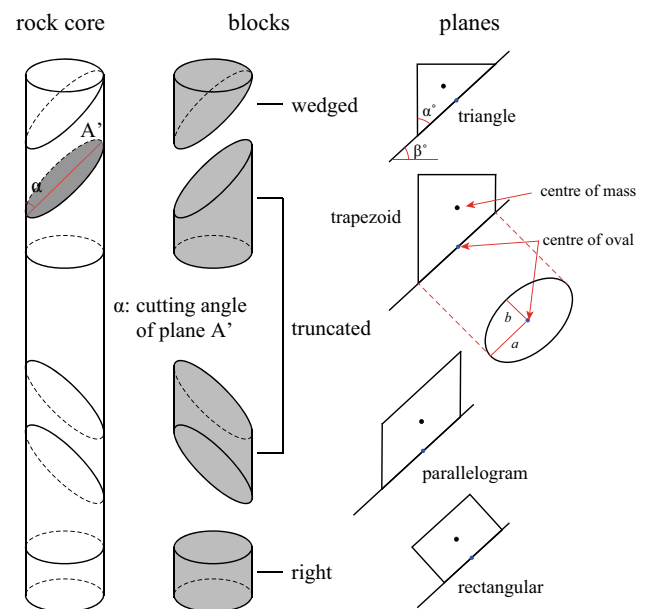


Fig. 1 Classification of the shapes of rock pieces along drilled cores

The sizes of the blocks also varied with the heights of the blocks according to the cutting positions.

2.2 Estimation of Normal Stress Distributions

2.2.1 Analytical Approaches

In tilt tests, the stress distribution of a block in the contact area of the tilt table changes according to the tilting angles, the shapes of the upper blocks, and the density distribution as the tilting table is inclined. Using a rectangular shape block, Hencher (1976) showed that the area of the leading edge of the block is more contacted than other regions and sliding is controlled by the joint surface in the region. When a plane is inclined, the stress distributions under a block change according to the angle of inclination, the geometry of the block, and the density of the block as shown in Fig. 2. Similar to the Hencher’s calculation about the rectangular block, the stress distributions of the categorized block shapes in the previous section are calculated based on a familiar analytic method for eccentrically loaded foundations (Das 2011). In this study, it is assumed that the nominal distribution of stress by a block is due to the vertical load combined with the subjected moments according to the location of the mass centre. As the cutting planes of core samples are circular and oval shapes, the vertical stresses at the contact areas can be expressed as Eqs. (1)–(3) based on the assumption of the case of circular foundation.

$$q = \frac{Q}{A} \pm \frac{M \cdot c}{I_y} \tag{1}$$

$$M = e \cdot Q \tag{2}$$

$$I_y = \frac{\pi a^3 b}{4} \quad (\text{ellipse}) \tag{3}$$

where M is the moment on the base; e is the eccentricity of the block shape; Q is the total vertical load; I_y is the moment of inertia about a rotational axis (y in Fig. 2b); $c = a$ (ellipse); a and b are radii of the major and minor axes of ellipse. Substituting Eqs. (2)–(3) into Eq. (1) gives

$$q_{\max}, q_{\min} = \frac{Q}{\pi ab} \left(1 \pm \frac{4e}{a} \right) \quad (\text{ellipse}) \tag{4}$$

The values of q_{\max} and q_{\min} are identified within the contact region (x). Generally, it is complicated to quantify the exact contact regions in accordance with the degree of tilt. In this study, the contact region is determined by the location of the eccentric load based on the effective area concept proposed by Meyerhof (1953) as given by Eq. (5). The contact region (x) and the corresponding effective area (a_e) vary with the angle of inclination as shown in Fig. 2c, d. For the rectangular shape cross section, normal stress is more likely concentrated towards the leading edge of the block reducing the effective area (see Fig. 2c). By contrast, in the case of trapezoid blocks, as the tilting table is inclined, the region of the stress distribution can be extended from the trailing edge to the leading edge of the

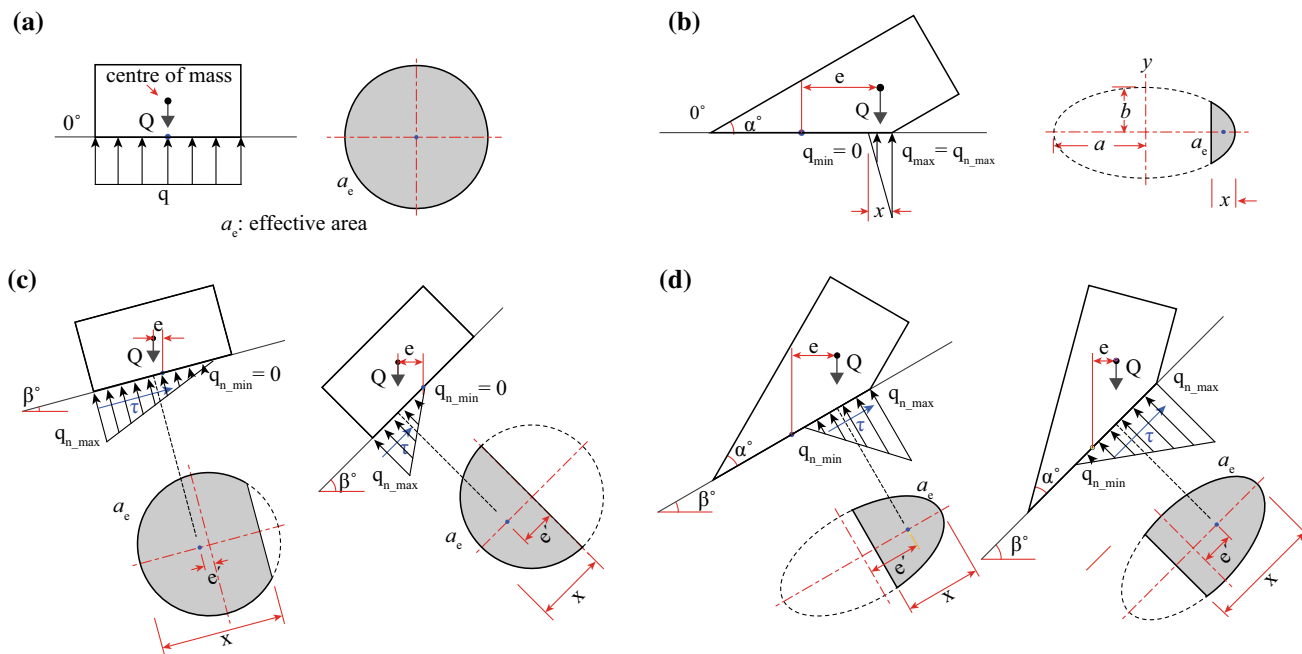


Fig. 2 Vertical stress distributions at the base of blocks with rectangular cross section (a), with trapezoid cross section (b); and normal stress distributions at the base of blocks as tilting table is inclined, with rectangular cross section (c), with trapezoid cross section (d)

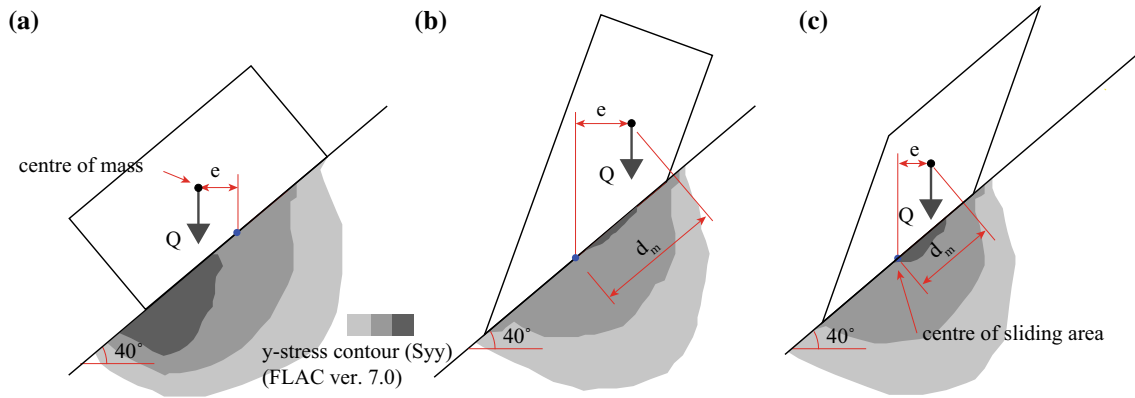


Fig. 3 y -stress contours at the base of the blocks, which were obtained using FEM analysis (FLAC ver. 7.0); rectangular (a), trapezoid (b), and parallelogram (c)

block due to the change in the directions of eccentric loads as shown in Fig. 2d.

In consideration of the variation in the effective areas (a_e), the vertical stresses q_{\max} and q_{\min} can be estimated by Eq. (6). In this range, the values of q_{\min} are negative when the eccentricities (e) are over $a/4$ (ellipse), which means that tensions are developed outside of the contact region (x). However, the negative values are ignored in this study as there is no tension between the block and the plane. The normal stress distributions at the base of blocks for the angles of inclination are simply calculated by using Eq. (7).

$$x = 2a - 2e' \quad (5)$$

$$q_{\max}, q_{\min} = \frac{Q}{a_e} \cdot \left(1 \pm \frac{4e'}{a}\right) \quad (\text{ellipse}) \quad (6)$$

$$q_{n_{\max}}, q_{n_{\min}} = q_{\max}, q_{\min} \cdot \cos \beta \quad (7)$$

where x is the effective width of the base and e' is the eccentricity of the tilted block; β is the tilting angle. The examples of normal stress distributions at the bases of blocks as tilting table inclined are demonstrated in Fig. 2c, d. As discussed above, the assumptions for the normal stress estimation in tilting conditions are established based on the influence of eccentric loading in accordance with the block shapes. In this study, the influence of the block shape on the normal stress is characterized by the locations of the centre of mass for the cross-sectional geometry of the blocks.

2.2.2 Numerical Analysis

In order to understand the differences in stress distributions, a numerical analysis was carried out using FLAC ver. 7.0 (Itasca 2011). The analysis focused on the simulation of the shapes of the stress distribution in the base of blocks when the blocks are located on the base. The geometries of the numerical models were created using the

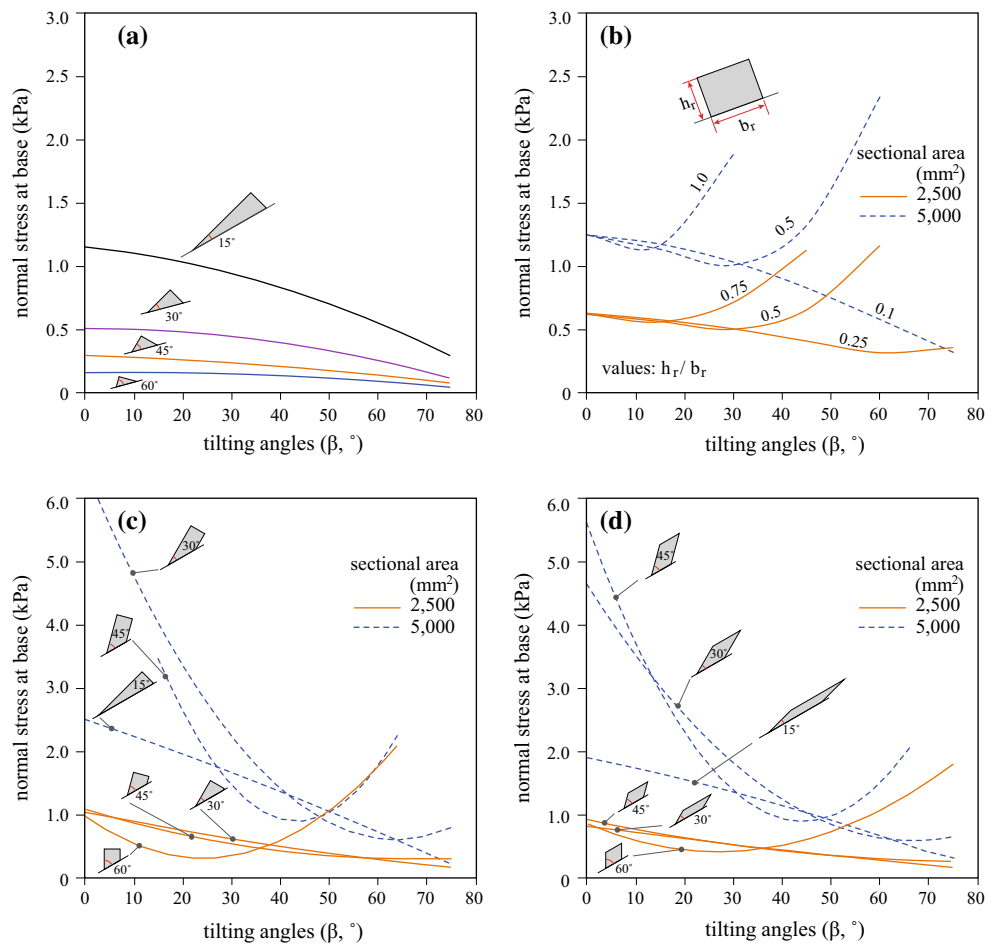
coordinates obtained from a rectangular model ($\alpha = 90^\circ$, $h_p = 50$ mm) and a parallelogram model ($\alpha = 30^\circ$, $h_p = 50$ mm) at a 40° angle of inclination. It should be noted that there are limitations in the ability of numerical models to simulate a stress distribution under a block using a finite element method. Firstly, the blocks are modelled as a part of the base with an elastic condition using a stiff modulus (1×10^8 kPa). Second, to obtain the overall stress distributions at the stage when the blocks are loaded on the base plane, the models are run for 100 cycles after the loading. Observation of the stress distribution at this stage confirmed the validity of this modelling. Figure 3 presents the geometries of the blocks and the y -stress contours in the base area.

The rectangular block, as shown in Fig. 3a, clearly shows the concentrated stress on the area of the leading edge compared to the parallelogram shape. This result agrees significantly with the theoretical findings obtained by Hencher (1976). The numerical analysis also shows that the stress contours of the truncated blocks (trapezoid and parallelogram) moved backward due to its centre of mass which was positioned close to the trailing edge. The positions of the 'centre of mass' of polygons vary with their shapes, and their locations can be identified using the distances from the centre of the joint plane. In this study, a parameter ' d_m ' can be defined as the horizontal distance of the centre of mass from the centre of the joint plane as shown in Fig. 3c.

2.2.3 Normal Stresses According to the Block Shapes and Tilting Angles

The shapes of stress distributions obviously vary according to the tilting angles. Relating the stress distribution with the geometries of blocks, it is interesting that ' d_m ' values can reflect the positions of stress contours because the truncated block has a larger ' d_m ' value than that of the

Fig. 4 Variations in normal stress at base in accordance with cutting angles and tilting angles, wedges (a), rectangular cross section (b), trapezoid (c) and parallelogram (d)



rectangular block (d_m is nil). In this study, the ‘normal stress at base’ is defined as the mean normal stress. So, the corresponding values were calculated by dividing the weight of the block at a given tilting angle ($Q \cos \beta$) by the effective sliding areas (a_e).

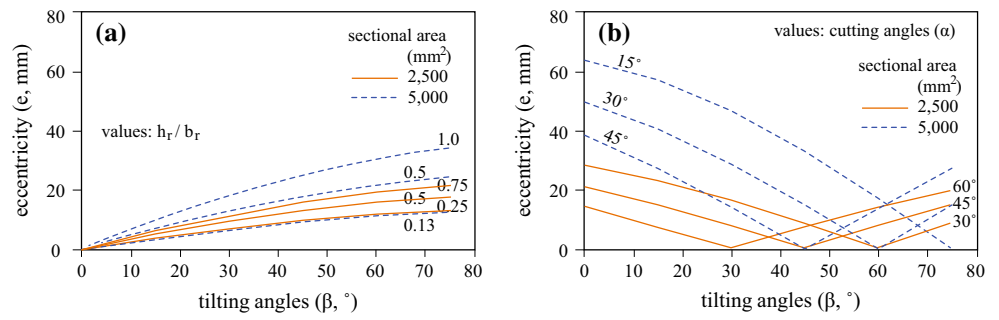
For the block shapes with four different cutting angles ($\alpha = 15, 30, 45, 60^\circ$) and for six different tilting angles ($\alpha = 0, 15, 30, 45, 60, 75^\circ$), the normal stresses at base were calculated using Eqs. (5)–(7). As the variations in the segment of an ellipse are not simply expressed by equations, the effective area of each case was directly obtained by measuring the area using AutoCAD.

Figure 4 demonstrates the normal stress variations for four different block shapes. The sizes of the blocks were divided into two groups (sectional area = 2500 and 5000 mm²), and the rectangular-, trapezoid-, and parallelogram-shaped blocks have equivalent sectional areas in each group. In a core cylinder, as the shapes of wedges have a whole circular plane at the end of the blocks, lower cutting angles produce sharper leading edges with larger volumes, as demonstrated in Fig. 4a. In all stress levels, the calculation results present consistent decreases in normal

stresses with increases in the angle of inclination. Compared to the rectangular sections (Fig. 4b), the stress reduction patterns of the wedges are similar given variations in cutting angles. As shown in Fig. 4b, for the blocks with rectangular sections, the normal stresses at the bases of the blocks are expressed using the ratio of height to width (h_r/b_r). It is demonstrated that the normal stress at the base can be raised as the tilting table is inclined according to the values of h_r/b_r . This is due to the increasing of eccentricity and the decreasing of effective area. The increase in normal stress is noticeable when h_r/b_r is over 0.5, as shown in Fig. 4b.

The normal stress of the blocks with trapezoid and parallelogram sections also decreased as the tilting angles are increased (Fig. 4c, d). The normal stress at base consistently decreases with increases in the tilting angle. It is shown that the stresses of the truncated blocks with large cutting angles also experience normal stress changes at an ascending rate. The transition of stress is directly related to the change in direction of eccentricity from the trailing edge to the leading edge. As a supportive description, Fig. 5 demonstrates the variations in the eccentricities of

Fig. 5 Variation in eccentricity of blocks with the angles of inclination, in accordance with the h_r/b_r ratio for rectangular shapes (a), in accordance with the cutting angles (α) for trapezoid shapes (b)



the block sections with variations in the angle of inclination. Compared to the steady increase in eccentricity for the rectangular shape sections, the blocks with trapezoid shape sections initially decrease in eccentricity and then increase after the transition points.

3 JRC Estimation

Using the results of tilt tests, JRC values can be estimated based on Barton’s empirical equation (Barton and Choubey 1977) as presented in Eq. (8).

$$JRC = \frac{\beta - \phi_b}{\log_{10} \left(\frac{JCS}{\sigma_{no}} \right)} \tag{8}$$

where ϕ_b is the basic friction angle of the joint; JCS is the compressive strength of the joint. To overcome the subjectivity of the visual observations, different roughness parameters have been employed to estimate JRC values using digitized 2D profiles (Tse and Cruden 1979; Maerz et al. 1990; Lee et al. 1990; Yu and Vayssade 1991). However, these roughness parameters have limitations for the accuracy of JRC estimations. Tse and Cruden (1979) proposed an empirical approach to estimate JRC values using Z_2 and SF which are the root mean square and the mean square of the first derivative of the profiles, respectively [Eqs. (9), (10)]. It was reported that Z_2 and SF show strong correlations with JRC values, and Z_2 shows better correlation with JRC values than SF (Yu and Vayssade 1991). The regressions were obtained from statistical analysis using 200 discrete amplitude measurements for every profile.

$$Z_2 = \left[\frac{1}{M(D_x)^2} \sum_{i=1}^M (y_{i+1} - y_i)^2 \right]^{1/2} \tag{9}$$

$$JRC = 32.2 + 32.47 \log Z_2 \tag{10}$$

where M is the number of intervals; D_x is a constant distance lag, and the sum of the squares in adjacent y-coordinates is divided by the product of the number of intervals. In this study, JRC values of natural core joint specimens

are estimated by Eqs. (9) and (10) using digitized roughness profiles obtained from a 1-mm interval profile gauge.

4 Experimental Procedure

4.1 Samples Used

A high-strength plaster material (Hydrocal) was used for making core shapes and rectangular shape joint sets. The strength of plaster is time-independent after the hardening process and its initial curing time are fast. Due to these advantages of using plaster in experiments, numerous studies have been performed to find the mixtures and mixing proportions to make stronger artificial samples which are more compatible for investigating behaviour of real rock specimens (Bandis et al. 1981; Indraratna 1990; Prombonas and Vlassidis 1994; Wibowo et al. 1995; Janeiro and Einstein 2010).

The plaster samples were made with water-to-cement ratios of 45 %, which was determined by considering workability for filling moulds. The samples were then cured in 30 °C oven temperature for 1 week to achieve harder specimens. The mixing ratio and curing condition of the plaster samples and the UCS test results are presented in detail (Kim et al. 2015). The properties of the specimens are presented in Table 1.

4.1.1 Core-Shaped Plaster Samples

As demonstrated in Fig. 6, a total of 18 core-shaped plaster samples were created with different dimensions based on three different shapes [wedged, truncated (trapezoid), and truncated (parallelogram)]. To simulate different stress levels, sample sizes were designed in three levels as presented in Table 2. The cutting angles (α) of the samples are 15°, 30°, and 45° in the same stress levels. PVC pipes (inner $\phi = 50$ mm, $t = 5$ mm) were used as the moulds of the samples. In each stress level, the sizes of the blocks were designed to create the same weights between the wedge or trapezoid shapes and the corresponding

Table 1 Properties of Hydrocal samples

Properties	Unit	Values	Notes
Specific gravity	–	2.96	–
Unit weight	kN/m ³	15.1–15.4	–
Unconfined compressive strength (UCS)	MPa	36.8–39.1	Cubic (100 × 100 × 100 mm)
Point load strength (I _{S(50)})	MPa	1.65–1.82	Cubic (50 × 50 × 50 mm)

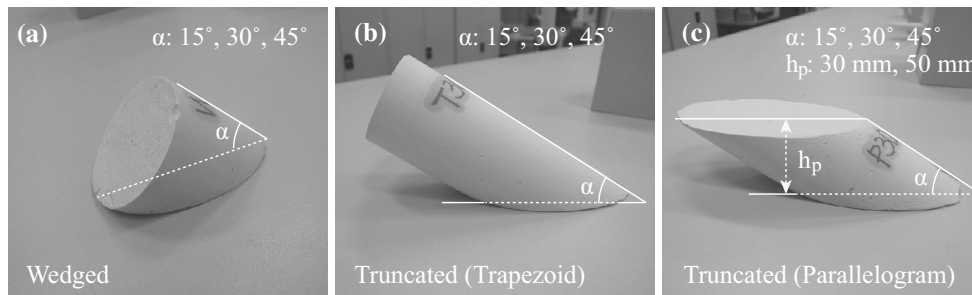


Fig. 6 Different shapes of plaster core pieces, with different sliced angles (α) and sample height (h_p)

Table 2 Normal stresses of the plaster core samples according to normal stress levels

Shapes	Stress levels								
	1			2			3		
Cutting angle, α , °	15	30	45	15	30	45	15	30	45
Wedged	302.8	148.3	78.9	–	–	–	–	–	–
Truncated (trapezoid)	–	–	–	381.0	202.9	127.5	609.1	308.3	214.9
Truncated (parallelogram)	316.9	156.8	85.3	372.1	185.4	135.9	562.6	293.1	206.1
Weight difference (%)	4.7	5.7	8.1	2.3	8.6	6.6	7.6	4.9	4.1

parallelogram shapes. The cured specimens were within 10 % of the differences in weights. For the measurement of basic friction angle, disc ($h = 30$ mm) and cylinder ($L = 100$ mm) shapes were also created following the standards of USBR 6258-09.

4.1.2 Rectangular Samples with Typical Roughness Profiles

Rectangular shape samples with different sample heights were created to investigate the sliding behaviour according to the roughness on joint planes. Barton’s typical roughness profiles were simulated on the matched joint sets. Four ranges of Barton’s roughness profiles (JRC = 0–2, 4–6, 8–10, 12–14) were simulated on the plaster samples. In order to simulate accurate roughness profile shapes, the coordinates of Barton’s typical roughness profiles were digitized in 1-mm intervals and were used to make 3D replicas using a 3D printing method. This procedure, as shown in Fig. 7, successfully created the plaster specimens with detailed roughness surface. For each replica set, the matched part was created by silicone to produce perfectly matched joint sets.

4.1.3 Natural Jointed Rock Cores

Six natural rock core samples were selected to investigate the effect of rock shapes in tilt tests. The rock types were shale and greywacke from the Brisbane area, and the geological and strength properties of the rocks were detailed in by Gratchev et al. (2013) and Kim et al. (2013). The roughness profiles of the samples were measured using a profile gauge with 1-mm interval step size. The roughness profiles were then digitized to estimate JRC values as shown in Fig. 8. JRC values were obtained using the roughness parameter, Z_2 and Eq. (7). The results are presented in Table 3. A series of Schmidt hammer tests were performed on the samples, resulting in the rebound values of 36–38 for the argillite and 32–38 for the greywacke specimens. The joint compressive strength (JCS) values were estimated using the mean values of the rebound data following Deere and Miller (1966).

4.2 Tilt Tests

A tilting test apparatus was designed to accommodate for both rectangular and core samples. As shown in Fig. 9,

Fig. 7 Procedure of sample preparation for jointed plaster samples using a 3D printer

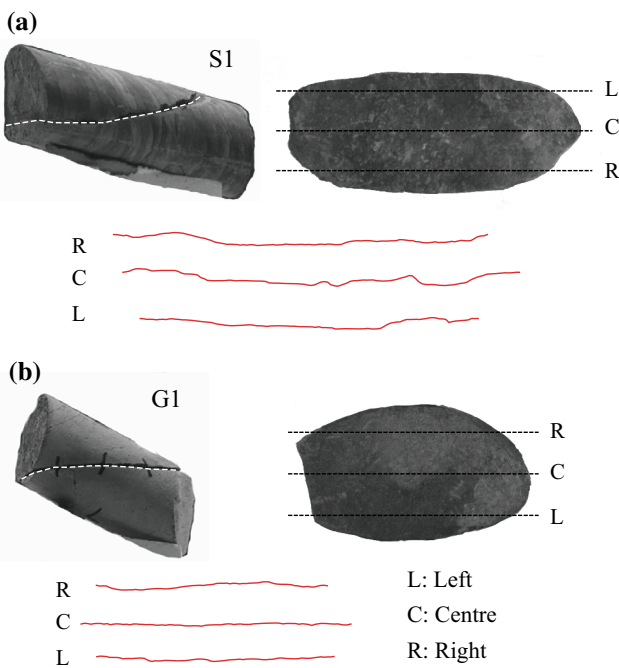
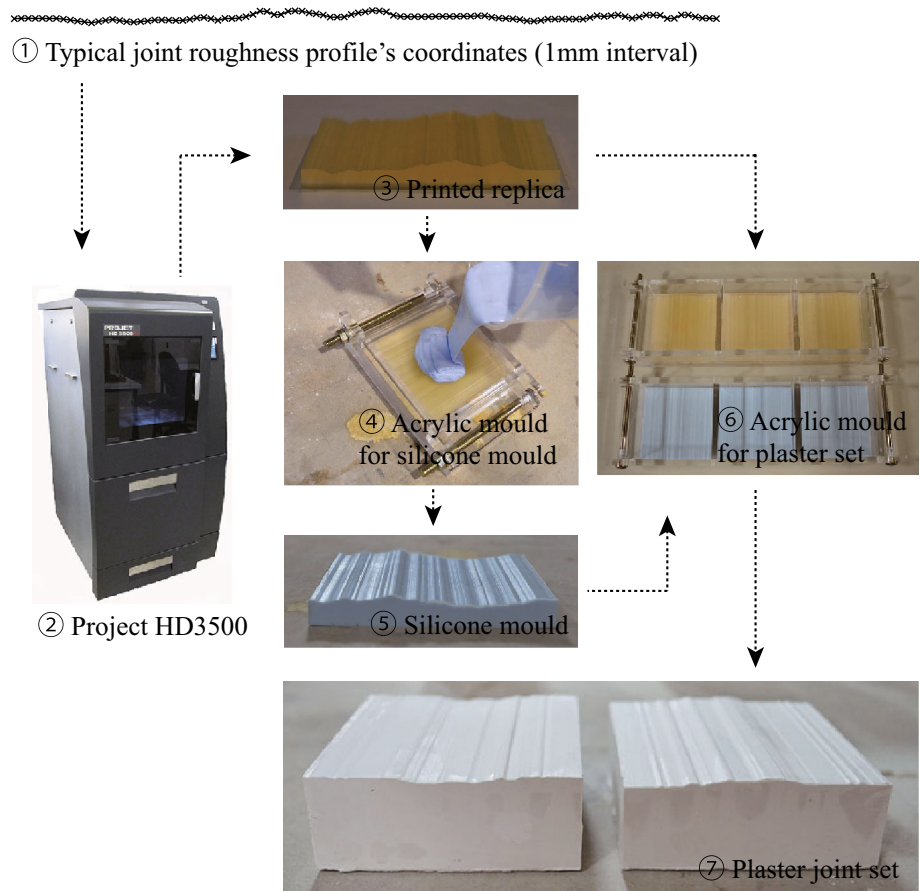


Fig. 8 Traced joint planes of upper core blocks and the roughness profiles along the planes: Shale, S1 (a), Greywacke, G1 (b)

tilting angles are directly measured by a digital tilt metre. Regarding the smooth tilting motion, the tilting table should be controlled with the rate less than 2.5° per minute to avoid any dynamic effects during tilting (USBR 6258-09). It is normally accepted that if the tilting rate is higher than this standard, the tilting angles at the sliding moment can be overestimated caused by dynamic influences. Bruce et al. (1989) compared the results of a set of tilt tests controlled by a motor at $2.5^\circ/\text{min}$ with the results at $8.0^\circ/\text{min}$ by both the motor and manual method. It is interesting from the results that a higher tilting rate and rotation by hand showed higher tilting angles, but the difference was insignificant. In this study, a screw handle, which can control the tilting rate less to than $2.5^\circ/\text{min}$, was developed to reach the sliding angles smoothly, thereby minimizing any dynamic influence.

4.2.1 Basic Friction Angles

Basic friction angles of Hydrocal samples and natural rock cores were measured using cylinder rock core specimens (height: 100–120 mm), following Stimpson's method

Table 3 Properties of rock core samples

Samples	Unit weight (kN/m ³)	Schmidt rebound (mean)	JCS (MPa)	JRC; L/C/R (mean)
Shale				
S1	28.9	36–38 (37.4)	86.5	8.2/13.3/8.9 (10.1)
S2				1.3/0.6/1.6 (1.2)
S3				2.9/5.2/3.5 (3.9)
Greywacke				
G1	28.0	32–38 (35.2)	71.5	4.6/3.6/5.6 (4.6)
G2				3.3/4.4/2.5 (3.4)
G3				1.5/3.3/2.7 (2.5)

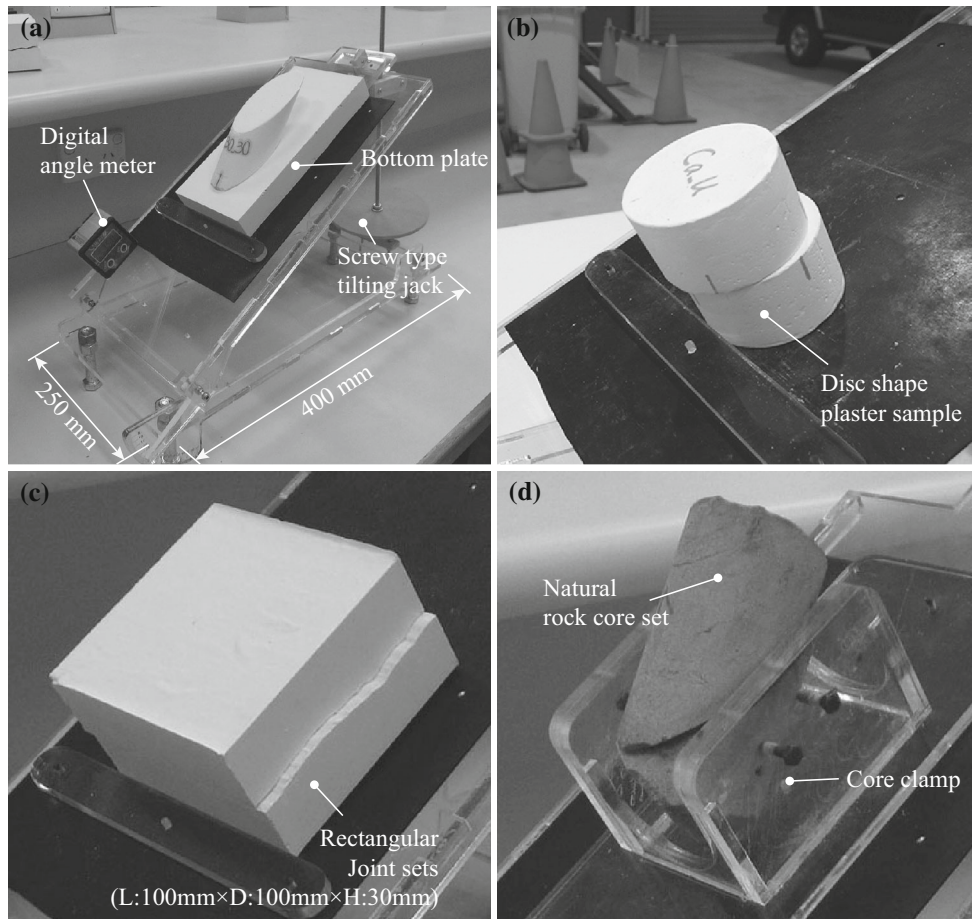


Fig. 9 Tilt test apparatus and test setup for sliced cores (a), disc samples for basic friction angle (b), rectangular samples (c), natural core joint sets (d)

(1981), and also disc specimens (height: 20–30 mm). Tilt tests were repeated 20 times for both specimens’ shapes.

In the case of rock core samples, the basic friction angles were calculated using the corrected formula (González et al. 2014), since the original equation is incorrect:

$$\phi_b = \tan^{-1}\left(\frac{\sqrt{3}}{2} \tan \beta\right) \tag{11}$$

where β is the inclination of the axis of cores and ϕ_b is the basic friction angle of rocks.

In this study, results indicated considerable differences between disc-type specimens and cylinder shape samples. The obtained mean values from disc-type samples were 38.1° of Hydrocal, 27.9° of Shale, and 28.8° of Greywacke. The mean values of basic friction angles using cylinder samples were 39.6° (Hydrocal), 37.4° (Shale), and 38.1° (Greywacke), respectively.

It had already been reported that Stimpson’s method tended to overestimate the basic friction angles. Alejano et al. (2012) showed that the friction angles obtained from

Table 4 Sliding angles (β) of core-shaped plaster samples

Stress levels	Block shape	Cutting angles (α , °)	Distance of centre of mass (d_m , mm)	Sliding angles (β , °)		
				Values	Mean	Standard deviation
1	Wedged	45	0.0	32.8–33.5	33.2	0.29
		30	8.3	38.6–39.5	39.1	0.37
		15	27.9	38.9–41.3	40.1	0.98
	Truncated—parallelogram ($h = 18$ – 24 mm)	45	8.8	37.6–38.3	38.0	0.29
		30	18.7	39.5–41.9	39.2	1.00
		15	45.1	40.5–42.2	41.6	0.70
2	Truncated—trapezoid ($h = 30$ mm)	45	17.9	41.3–43.4	42.2	0.88
		30	32.2	41.6–43.9	42.7	0.94
		15	71.0	43.5–45.0	44.1	0.65
	Truncated—parallelogram ($h = 30$ mm)	45	15.0	38.1–38.3	38.2	0.08
		30	26.0	38.8–39.6	39.2	0.33
		15	56.0	41.1–42.4	41.6	0.59
3	Truncated—trapezoid ($h = 50$ mm)	45	27.9	36.6–37.8	37.2	0.49
		30	49.5	40.0–42.1	41.0	0.87
		15	108.3	43.3–44.7	44.2	0.64
	Truncated—parallelogram ($h = 50$ mm)	45	17.7	38.7–39.2	39.0	0.21
		30	43.3	39.6–41.2	40.4	0.65
		15	93.3	42.2–42.6	42.4	0.17

the Stimpson method were much greater than the values obtained from disc-type samples. They referred that the increase is mainly due to the different sliding behaviour between the generatrices of core samples and the plane surfaces of disc samples.

4.2.2 Influence of Block Shapes on Tilting Angles

Using the core-shaped plaster samples, tilt tests were performed ten times for each sample. The obtained sliding angles showed a small data deviation range $<1^\circ$, as summarized in Table 4. Wedged blocks slid at low tilt angles, and truncated blocks (trapezoid) showed larger tilt angles than other shapes. The results demonstrated that the tilting angles (β) at the sliding moment increase with ' d_m ' values, as demonstrated in Fig. 10.

At the lowest normal stress level, the wedges and the corresponding truncated (parallelogram) blocks slid in a low range of tilting angles from 33° to 40° . In this range, the truncated blocks create higher tilting angles than the wedges due to their larger ' d_m ' values. The differences in tilting angles between the trapezoid- and parallelogram-shaped blocks are apparent in the next stress level (dotted cubic and circle marks in Fig. 10). Because the trapezoid shapes have larger ' d_m ' values, the blocks are slid at higher tilting angles than the corresponding parallelogram shapes. However, this trend is diminished as

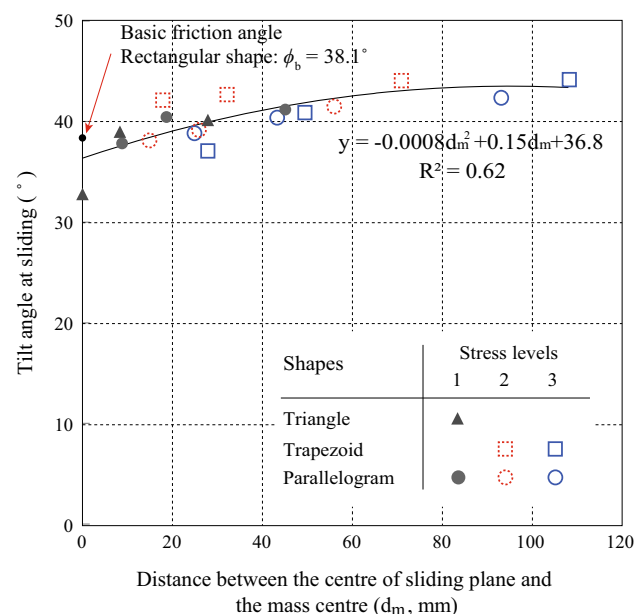


Fig. 10 Distribution of basic friction angles according to the ' d_m ' values of block shapes

the stress levels increase. In the third stress levels (closed cubic and circle marks in Fig. 10), the differences in the tilting angles between both shapes were reduced.

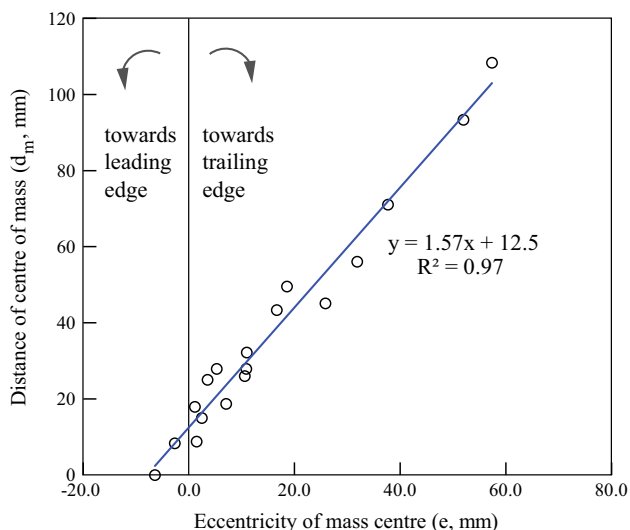


Fig. 11 Correlation between eccentricities of mass centres and ‘ d_m ’ values

The relationship between the tilt angles at sliding moments and the ‘ d_m ’ values of all data formed an inclined regression curve, which is due to the differences in the mass centres of block shapes. As discussed in Sect. 2.2, the eccentricities of mass centres are related to the variations in normal stress at the base of tilting blocks. The correlation between the eccentricities at their tilting angles and the ‘ d_m ’ values of the samples is clearly identified as shown in Fig. 11. Both eccentricities and ‘ d_m ’ values significantly agreed with each other, showing a linear regression in all stress levels. In the data, a negative eccentricity indicates the moment towards the leading edge of the block.

The measurement of basic friction angles (ϕ_b) is influenced by the block shapes. The results of the plaster samples indicate that the basic friction angle of the plaster blocks can be estimated by the parameter ‘ d_m ’ values, as presented in Fig. 10. The basic friction angle is an

influential factor in determining JRC values. Based on this result, this study suggests the use of the corresponding basic friction angles according to the employed block shapes in tilt tests for JRC estimation. The normal stress variations according to the block shapes can also be applied for improving JRC estimation. In the case of the four block shape categories in Fig. 4, the normal stress variations were determined by the reduction ratio in accordance with tilting angles. As demonstrated in Fig. 12, the regression curves present different patterns associated with their modes of normal stress distributions. The shapes of the stress reduction curves can be expressed by quadratic functions, except for the cases of sharp increases in normal stress. The wedge-shaped blocks show a downward trend, either in a convex or concave shape, depending on their cutting angles as shown in Fig. 12a. The truncated blocks demonstrate an overall downward trend in a concave manner, and the trends are similar between the trapezoid and the parallelogram shapes. The slopes of the curves are changed by the cutting angles. The basic form of the curves is given by Eq. (12).

$$\sigma_n = c_1\beta^2 + c_2\beta + c_3 \tag{12}$$

where ‘ c_1 ’, ‘ c_2 ’, and ‘ c_3 ’ are coefficients to determine the direction, the slopes, and the location of the vertex of the curves. The coefficients of the regression curves are summarized in Table 5.

4.2.3 Limitation of JRC Values on Tilt Tests

The matched rectangular joint sets, which are simulated with Barton’s typical roughness profiles, showed a large tilt angle ranging from 35° to 68° as summarized in Table 6. The tilt tests were performed for both directions of the employed roughness profiles and repeated 30 times for each direction, while considering the data deviations due to the irregularity of the sliding surfaces. JRC values were

Fig. 12 Normal stress reduction ratio according to block shapes, wedges and truncated blocks (a), rectangular section blocks (b)

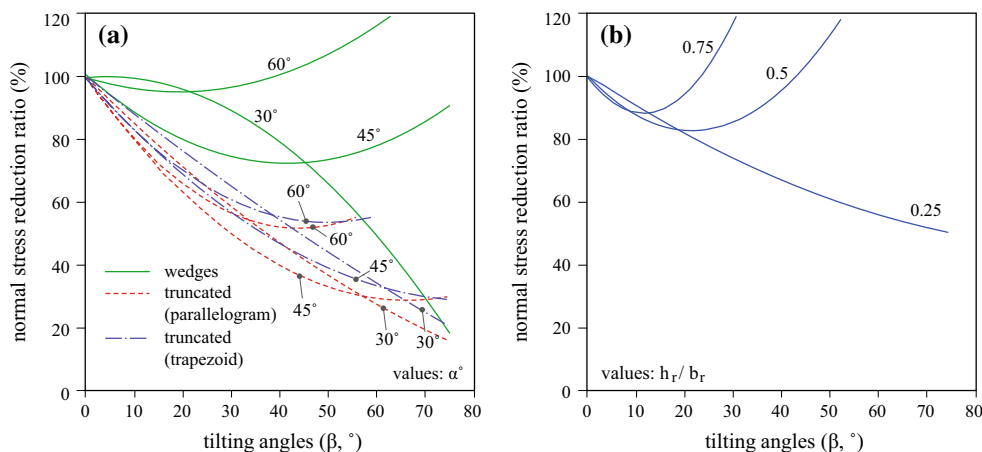
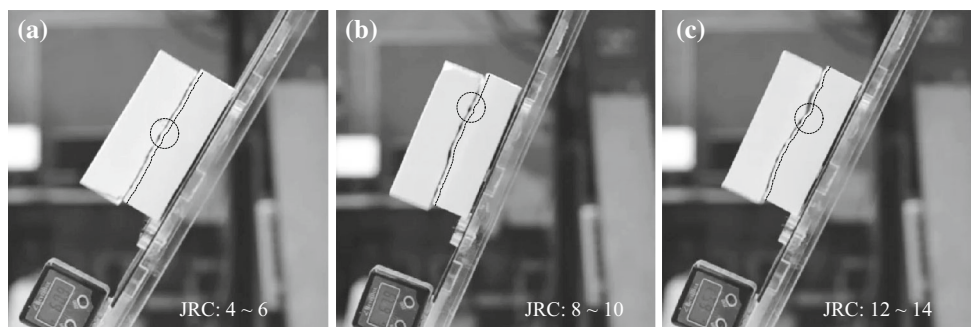


Table 5 Coefficients of the stress reduction curves

Block shapes	Cutting angles (α , °)	Coefficients			Coefficient of determination, R^2
		c_1	c_2	c_3	
Wedged	30	-0.0166	0.1464	103.2	0.99
	45	0.0166	-1.3739	99.9	0.76
	60	0.0128	-0.4929	100.1	0.98
Truncated (trapezoid)	30	0.0058	-1.56	101.5	0.99
	45	0.0163	-2.1565	99.7	0.98
	60	0.0251	-2.2076	97.7	0.93
Truncated (parallelogram)	30	0.0024	-1.2364	100.5	0.99
	45	0.0106	-1.7363	99.2	0.98
	60	0.0186	-1.8512	97.9	0.93
Rectangular (h_r/b_r : 0.25)	-	0.0047	-1.0288	103.0	0.94

Table 6 Tilting angles (β) of rectangular jointed plaster sets

JRC (on samples)	Tilting angles (β , °)			JRC (σ_n : normal)	JRC (σ_n : corrected)
	Values	Mean	SD		
0–2 (flat)	35–46	40.2	1.78	-1.0 to 2.6 (mean: 0.7)	-1.0–2.5 (mean: 0.7)
4–6	58–65	61.6	2.24	6.7–9.1 (mean: 8.0)	6.2–8.2 (mean: 7.3)
8–10	62–72	67.5	2.87	8.1–11.5 (mean: 10.0)	7.4–10.1 (mean: 8.9)
12–14	65–77	70.2	3.26	9.1–13.2 (mean: 10.9)	8.2–11.2 (mean: 9.6)

**Fig. 13** Captured images at sliding moment and observed trigger asperities for sliding: JRC = 4–6 (a), 8–10 (b), 12–14 (c)

back-calculated using Eq. (8). In this equation, normal stresses were calculated using the suggested shape correction function, as given in Eq. (12).

The calculations were dependent on the case of a rectangular foundation based on an eccentric loading (Das 2011) as discussed in Sect. 2.2.1.

In the low JRC ranges (<8–10), tilt tests generally overestimated JRC values. However, the suggested shape correction function for normal stress can reduce the JRCs reasonably compared to the traditional method. In the high JRC ranges (more than 8–10), it was observed that the upper sets in tilt tests did not slide smoothly because of the partial interlocked asperities on the sliding surfaces (see Fig. 13). These pictures were traced from the recordings of

tilt tests using a digital camera (in 0.125 s). This conclusion agrees reasonably well with Barton's experiments. Barton suggested a range of tilt test applications in which the surfaces of rock joints should be smooth enough to avoid toppling failure in the sliding location. The JRC range (8–10) was thus suggested as the maximum limit of JRCs for tilt tests.

4.2.4 Application of Shape Factors on Tilt Tests Using Natural Rock Core Samples

Using the natural rock specimens of core joints, tilt tests were performed 20 times for each block. The dimensions of the upper blocks and the joint surfaces were measured as

Table 7 Dimensions of natural rock core joint sets and tilt test results

Sample dimensions	Samples					
	S1	S2	S3	G1	G2	G3
α (°)	16.0	14.0	7.0	32.0	16.0	9.0
d_m (mm)	10.0	2.7	8.9	17.0	15.5	3.0
h_m (mm)	19.0	17.6	6.3	18.6	12.2	8.1
Joint area (mm ²)	5589	4252	3767	3872	6425	4532
Weight of upper block (g)	345	227	118	242	326	153
σ_n (kPa)						
Normal	6.2	5.4	3.2	6.3	5.1	3.4
Corrected	3.5	4.5	2.2	2.7	2.9	2.8
Basic friction angle (°)	27.9	27.9	27.9	28.8	28.8	28.8
JRC						
Measured	10.1	1.2	3.9	4.6	3.4	2.5
Normal	5.6	0.7	5.8	6.6	5.1	2.4
Corrected	5.2	0.6	5.5	5.9	4.7	2.4

shown in Table 7. The core pieces are wedges, and the centres of mass are located near the trailing edges of the blocks. Measured JRC values are compared with calculated values in Table 7. It was found that when ' d_m ' values are relatively large (S3, G1, G2), the calculated JRC values were overestimated. However, for the S1 sample, tilt tests underestimated the JRC value. This result is in close accord with the limitation of tilt tests for high JRC ranges, as mentioned in the previous section. It is interesting that S2 and G3 samples, which have small ' d_m ' values, showed considerably lower tilting angles. It was found that the sliding angles in several trials were smaller than those of the basic friction angles. With consideration of the ' d_m ' values, the low tilting angles were due to the small ' d_m ' values.

Regarding the influence of the shape factor, JRC values were also back-calculated using the shape correction functions for basic friction angles and normal stresses. For example, the shape of the shale block, S3, was first identified using the measured ' d_m ' value ($d_m = 8.9$). Using the normal stress reduction curves in Fig. 12, the normal stress at the sliding moment was then estimated. The application results of the shape correction factors show that the suggested shape functions of normal stresses can reduce the differences between measured JRCs and back-calculated JRCs. In summary, the suggested shape functions could improve the accuracy of the estimation, considering the shape effect of the samples. However, it should be noted that the suggested functions were totally based on the results from plaster samples; the differences can be more reasonably improved by using the results from the tests of real rock samples in any subsequent studies.

5 Conclusion

The influences of sample shapes on normal stress and friction angles are analytically and experimentally investigated in this study. Based on the results of normal stress distribution analysis, normal stress correction functions are proposed for JRC estimation using tilt tests. Using a variety of artificial and natural samples, a series of tilt tests was performed to clarify the influences of the sample shapes. Based on the obtained results, the following conclusions can be drawn:

- Wedged, truncated (trapezoid- and parallelogram-shaped), and rectangular shapes were employed as the probable shapes of core specimens for tilt tests.
- The ' d_m ' parameter, which is the horizontal distance between the mass centre and the centre point of sliding plane, directly indicated the relationship between the sliding angles and the block shapes.
- Tilting angles at the point of sliding increased with increasing values of ' d_m '. Using the relationship between the increased tilting angles and the corresponding ' d_m ' values, a regression curve was suggested. This regression represents the variation in basic friction angles with different block shapes.
- The limitation of the use of tilt tests for JRC estimation was defined by the JRC <8–10 through a set of tilt tests using rectangular shape plaster samples with simulated Barton's typical roughness profiles.
- The normal stress reduction functions were proposed to account for the effect of the normal stress distribution. These functions can reduce the deviations in measured values for natural rock core samples and plaster joint sets.

Acknowledgments This research was performed with the financial support of the Griffith University International Postgraduate Research Scholarship (GUIPRS) program. The authors would like to express their appreciation to anonymous reviewers for the constructive comments which have contributed to improved research and, consequently, outcomes.

References

- Alejano LR, Gonzalez J, Muralha J (2012) Comparison of different techniques of tilt testing and basic friction angle variability assessment. *Rock Mech Rock Eng* 45:1023–1035
- Bandis S, Lumsden AC, Barton N (1981) Experimental studies of scale effects on the shear behaviour of rock joints. *Int J Rock Mech Min Sci Geomech* 18:1–21
- Barton NR (2008) Shear strength of rockfill, interfaces and rock joints, and their points of contact in rock dump design. In: *Proceedings of Rock dumps 2008*, Perth, pp 3–18
- Barton N, Bandis S (1980) Some effects of scale on the shear strength of joints. *Int J Rock Mech Min Sci Geomech Abstr* 17:69–73
- Barton N, Choubey V (1977) The shear strength of rock joints in theory and practice. *Rock Mech* 10:1–54
- Baumgartner P, Stimpson B (1979) Development of a tiltable base friction frame for kinematic studies of caving at various depths. *Int J Rock Mech Min Sci Geomech* 16:265–267
- Bray JW, Goodman RE (1981) The theory of base friction models. *Int J Rock Mech Min Sci* 18:453–468
- Bruce IG, Cruden DM, Eaton TM (1989) Use of a tilting table to determine the basic friction angle of hard rock samples. *Can Geotech J* 26:474–479
- Cawsey DC, Farrar NS (1976) A simple sliding apparatus for the measurement of rock joint friction. *Géotechnique* 26(2):382–386
- Das BM (2011) *Principles of foundation engineering*, 7th edn. Cengage Learning, Stanford
- Deere DU, Miller RP (1966) Engineering classification and index properties for intact rocks. *Tech. Report*. Air Force Weapons Lab., New Mexico, No. AFNL-TR: 65-116
- González J, González-Pastoriza N, Castro U, Alejano LR, Muralha J (2014) Consideration on the laboratory estimate of the basic friction angle of rock joints. In: *Proceedings of the 2014 ISRM European Rock Mechanics Symposium (EUROCK 2014)*, Vigo, Spain, pp 199–204
- Gratchev I, Shokouhi A, Kim D, Stead D, Wolter A (2013) Assessment of rock slope stability using remote sensing technique in the Gold Coast area, Australia. In: *Proceedings of the 18th Southeast Asian Geotechnical & Inaugural AGSSEA Conference*, pp 729–734
- Hencher SR (1976) Discussion on a simple sliding apparatus for the measurement of rock joint friction. *Géotechnique* 26:641–644
- Indraratna B (1990) Development and applications of a synthetic material to simulate soft sedimentary rocks. *Géotechnique* 40(2):189–200
- ISRM (1978) Suggested methods for the quantitative description of discontinuities in rock masses. *Int J Rock Mech Min Sci Geomech Abstr* 15:319–368
- Itasca consulting group Inc. (2011) *Fast Lagrangian analysis of continua user's guide*. Minneapolis
- Janeiro RP, Einstein HH (2010) Experimental study of the cracking behaviour of specimens containing inclusions (under uniaxial compression). *Int J Fract* 164:83–102
- Kim DH, Gratchev I, Balasubramaniam AS (2013) Determination of joint roughness coefficient (JRC) for slope stability analysis: a case study from the Gold Coast area, Australia. *Landslides* 10:657–664
- Kim DH, Gratchev I, Balasubramaniam AS, Chung M (2015) Determination of mobilized asperity parameters to define rock joint shear strength in low normal stress conditions. In: *Proceedings of the 12th ANZ conference on geomechanics*, Wellington, New Zealand, pp 1145–1152
- Lee YH, Carr JR, Barr DJ, Haas CJ (1990) The fractal dimension as a measure of the roughness of rock discontinuity profiles. *Int J Rock Mech Min Sci Geomech Abstr* 27:453–464
- Maerz NH, Franklin JA, Bennett CP (1990) Joint roughness measurement using shadow profilometry. *Int J Rock Mech Min Sci Geomech* 27:329–343
- Meyerhof GG (1953) The bearing capacity of foundations under eccentric and inclined loads. In: *Proceedings of the 3rd International Conference on Soil Mechanics and Foundation Engineering (ICSMFE)*, Zürich, vol 1, pp 440–445
- Norwegian Geotechnical Institute (2004) Forsmark site investigation, Borehole: KFM04A, Tilt testing. *Technical report*, SKB P-04-179, ISSN 1651-4416
- Prombonas A, Vlassidis D (1994) Compressive strength and setting temperatures of mixes with various proportions of plaster to stone. *J Prosthet Dent* 72(1):95–100
- Sagaseta C (1986) On the modes of instability of a rigid block on an inclined plane. *Rock Mech Rock Eng* 19:261–266
- Stimpson B (1981) A suggested technique for determining the basic friction angle of rock surfaces using core. *Int J Rock Mech Min Sci Geomech* 18:63–65
- Tse R, Cruden DM (1979) Estimating joint roughness coefficients. *Int J Rock Mech Min Sci Geomech Abstr* 16:303–307
- USBR 6258-09 Procedure for determining the angle of basic friction (static) using a tilting table test
- Wibowo J, Amadei B, Price RH, Brown SR, Sture S (1995) Effect of roughness and material strength on the mechanical properties of fracture replicas. SANDIA report, SAND94-1941, Sandia national laboratories, California 94550 the United States
- Wines DR, Lilly PA (2003) Estimates of rock shear strength in part of the Fimiston open pit operation in Western Australia. *Int J Rock Mech Min Sci* 40:929–937
- Yu X, Vayssade B (1991) Joint profiles and their roughness parameters. *Int J Rock Mech Min Sci Geomech Abstr* 24(4):333–336